Random sequential adsorption of parallel squares

Benjamin J. Brosilow, Robert M. Ziff, and R. Dennis Vigil
Department of Chemical Engineering, The University of Michigan, Ann Arbor, Michigan 48109-2136
(Received 4 June 1990; revised manuscript received 10 September 1990)

The random sequential adsorption of parallel (aligned) squares is studied by computer simulation. A new precise value of the maximum (jamming) coverage is found: $\theta_J = 0.562\,009 \pm 0.000\,004$. The dynamics for times $t \gtrsim 6000$ agree with Swendsen's prediction $\theta_J - \theta(t) \sim c(\ln t)/t$. Various two-point correlation functions are measured, and the effects of the finite size and the discretization of the adsorbing surface are also investigated.

I. INTRODUCTION

Random sequential adsorption (RSA) is a model for the irreversible adsorption of objects on a surface. In the simplest form of RSA, the objects have no interaction other than a hard repulsion that prevents overlap between particles. An adsorption site is chosen at random, and a new object is placed there only if it does not overlap any previously adsorbed object. A rejected object is assumed to completely randomize its position before it tries to adsorb again. The latter assumption makes the model conceptually simple and absent of any parameters except for the shape of the adsorbing object and, in finite systems, the size and shape of the adsorbing surface.

RSA is a fundamental model of irreversible behavior and is thus of broader interest than just for the study of adsorption. RSA was first proposed as a model of random packing in three dimensions (to describe the state of a liquid) by Bernal,[1] and his interest stimulated much of the early work. RSA is also used routinely to generate a "random" configuration of particles to initialize a Monte Carlo simulation (for systems of sufficiently low density).

In one-dimensional systems, RSA has been solved analytically in both discrete[2,3] and continuous cases.[4] In higher dimensions asymptotic theoretical results have been derived,[5–7] and formal expansions exist[8] which produce uniformly accurate results after resummation.[9] Computer simulations have been performed in two dimensions for the adsorption of disks,[7,10,11] parallel squares,[6,12–16] randomly oriented ellipses,[17] and randomly oriented rectangles[18] on a continuum surface, and squares[19] and more intricate shapes[20,21] on a discrete lattice have been investigated. Computer simulations on aligned hypercubes in higher dimensions have also been carried out.[15] Some other recent papers that consider various interesting aspects of the RSA problem are listed in Refs. 22–25.

Here we are concerned with the problem of RSA of a system of parallel squares (in which the edges of the different squares are aligned parallel to each other), adsorbing on a continuum two-dimensional surface. This system is also called oriented squares, or aligned squares. The interest in RSA of parallel squares originated with a conjecture of Palásti[26] that the maximum coverage θ_J for squares in two dimensions is exactly the square of the maximum coverage for segments in one dimension, $\theta_J^{(1)}$,

$$\theta_J = (\theta_J^{(1)})^2 \approx 0.558\,902\,650\,4 , \tag{1}$$

where

$$\theta_J^{(1)} = \int_0^\infty e^{-2f(x)} dx \approx 0.747\,597\,920\,253\,38 , \tag{2}$$

and

$$f(x) = \int_0^x (1-e^{-y}) y^{-1} dy = E_1(x) + \gamma + \ln x$$

Here $E_1(x)$ is the exponential integral function and γ is Euler's gamma constant.[27] While early numerical work tended to find agreement with (1),[6,13] more precise measurements of θ_J showed (1) to underestimate the actual value of θ_J by about 0.5%.[12,14,15]

Besides the question of the coverage of the jamming limit, the dynamics are an important aspect of RSA. Time t is defined as the number of adsorption trials (successful or not) per unit area, with the unit of area taken to be equal to the area of a single adsorbing particle. Swendsen[16] has given theoretical arguments indicating that for parallel squares the asymptotic time behavior of the coverage as the jamming limit is approached should be given by

$$\theta_J - \theta(t) \sim c(\ln t)/t , \tag{3}$$

where c is a constant. Note $\theta(\infty) = \theta_J$. This behavior is in contrast to that of disks, where $\theta(t)$ satisfies Feder's law,[11]

$$\theta_J - \theta(t) \sim c' t^{-1/2}, \quad t \to \infty \tag{4}$$

and randomly oriented rectangles[18] and ellipses,[17] where $\theta(t)$ satisfies

$$\theta_J - \theta(t) \sim c'' t^{-p}, \quad t \to \infty \tag{5}$$

with $p \leq \frac{1}{2}$. The value of p depends on the shape of the adsorbing particle.[17,18]

Theoretical arguments in support of (4) have been given by Swendsen[16] and Pomeau,[5] and extended by Hinrichsen, Feder, and Jøssang,[7] and arguments in support

of (5) have been given by Talbot, Tarjus, and Schaaf.[17] The reason that the behavior of parallel squares is different from that of disks is that for parallel squares the regions of the surface in which adsorption can occur at the late states of the process remain as rather large rectangles, while for disks they become very small triangle-shaped regions.[16] For randomly oriented rectangles and ellipses, the kinetics is slowed further by orientational constraints.

We note that parallel squares have also been studied extensively in the context of a gas in equilibrium, using virial expansions[28] and by Monte Carlo simulation.[29] However, it is well known that RSA is equivalent to equilibrium systems only in the zero-density (or -coverage) limit.[8,30]

Our motivation for reexamining the parallel-square model stemmed from the fact that this model can be simulated all the way to the jamming limit using a relatively small amount of computer time. Hence, we were able to collect data on this model that are considerably more accurate than the data available for any other currently studied RSA model in two (and higher) dimensions. With these data we were able to study many aspects of the process in detail.

II. THE ALGORITHM

A. Adsorption of squares

We consider a surface of size 256×256, where the unit of length is equal to the edge of a single adsorbing square. This surface is divided into 256×256 cells of unit area, so that at most only one center of a square can fall within each cell, as shown in Fig. 1. To adsorb a new square, a cell is chosen at random, and, if the cell is empty, then x and y coordinates are generated within the unit cell. The adsorption of a new square centered at these coordinates is accepted if there is no overlap with squares in neighboring cells. The overlap condition is simply $|\Delta x|<l$ and $|\Delta y|<l$, where l is the side of a square (here taken to be unity). This part of the algorithm is similar to the method of Akeda and Hori.[13]

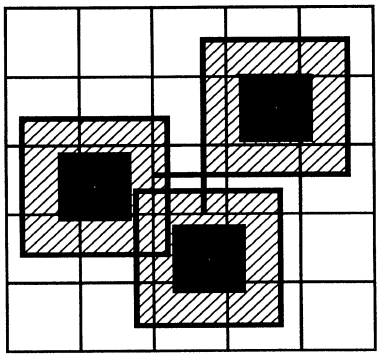

FIG. 1. Three squares (black) adsorbed on a 5×5 section of the surface. The surface section is shown divided into 25 "cells" of unit area, as discussed in the text. The hatched regions around each square show the "excluded area," onto which the adsorption of additional square centers is prohibited. The central cell on the 5×5 surface is shown divided into a lattice of nine rectangles, three of which are available for further adsorption of squares centers, and six of which are blocked.

Eventually, there will be cells that are empty yet completely blocked from adsorption because of squares in neighboring cells. (At jamming, the fraction of such blocked cells is just $1-\theta_J$.) We developed an algorithm that determines those blocked cells as follows: For each cell, the eight surrounding nearest-neighbor and next-nearest-neighbor cells are checked. Squares in any of these eight cells will block out a region in the central cell where there can be no adsorption, as shown in Fig. 1. Squares in the nearest-neighbor cells will block out a region (in the central cell) to one side of a line (horizontal or vertical), while those in the next-nearest-neighbor (corner) cells will block out a corner region bounded by vertical and horizontal lines. These vertical and horizontal lines divide the central cell into a lattice of rectangles. The program first determines all these lines and thus defines the lattice, and then it determines which rectangular regions within the lattice are blocked and which are free for adsorption. If all the regions are blocked, then the cell is marked as such, and adsorptions are no longer attempted on these cells.

In the late stages of the program, when there are a relatively small number of unblocked rectangular regions left, those rectangles are put on a list (maximum length 256) and adsorption is carried out only in them. A given rectangle is chosen with a probability proportional to its area, and then a point is chosen randomly within that area. The jamming limit is finally reached when there are no more free rectangles left to adsorb a square.

B. Time dependence

In the initial stage of the algorithm, sites onto which adsorptions are attempted are chosen randomly from the entire surface of area $A=256\times256$. In this initial stage, the time is incremented by $\Delta t=1/A$ after each adsorption attempt. In the later stages of the algorithm, however, the sites onto which adsorptions are attempted are chosen only from a subset of the area A, as described in the preceding subsection. The time increment between adsorptions for these later stages was calculated as

$$\Delta t=\frac{\mathrm{int}[\ln R/\ln(1-\beta)]+1}{A}\ , \tag{6}$$

where β is the fractional area of the surface in which adsorptions are attempted, R is a uniformly distributed random variable $0<R\le1$, and $\mathrm{int}[x]$ is the function whose result is the integer part of x. Equation (6) is defined such that $P(\Delta t)=\beta(1-\beta)^{A\Delta t-1}$ is the probability that the time interval between two adsorption attempts will equal Δt (where $A\Delta t$ is the number of trials, and is an integer). With this method of incrementing the time, the simulation is exactly equivalent to a true RSA process, where adsorption sites are chosen at random from the entire surface of area A throughout the adsorption.

C. Discussion

We found that jamming generally occurred by $t \approx 2^{31}$. Had we continued with the naive approach of choosing cells randomly (which was used in the early stages of the program), we could not have reached the jamming limit even once in the computing time available to us. A simulation using only the simple adsorption procedure required several days of computer time to reach $t = 2^{15}$. This means that every cell was tried $2^{15} = 32\,768$ times, yet there were still roughly eight adsorptions to go before jamming. Several thousand ($> 2^{16}$) days of computer time would have been needed to reach the jamming limit this way.

We note that Jodrey and Tory[15] developed a related procedure for simulating RSA of parallel squares to the jamming limit. In their procedure, they created a linked list to record the vertices of the graph that is formed by all the rectangles in the system, and then they adsorbed only in the free rectangles. After each adsorption, new vertices were created. Periodic boundary conditions were used, and the program was generalized for 1–4 dimensions. While their method is efficient in that a square is adsorbed after each attempt, the bookkeeping appears to be rather time consuming. The same method was used for the entire simulation. In contrast, our program used different techniques at three distinct stages to improve both speed and storage efficiency, with the time- and memory-consuming adsorption in individual rectangles done only at the end when the size of those rectangles is very small. Jodrey and Tory adsorbed a total of just over 2×10^6 squares on a series of lattices as large as 100×100, consuming ≈ 27 h of IBM 370/158 central-processing-unit time. Their result, $\theta_J = 0.562\,10 \pm 0.000\,28$, was the most precise before the present work.

Hinrichson *et al.*[7,11] have developed a procedure for simulating RSA to the jamming limit for the case of disks. In their procedure, they identify the Voronoi-Dirichlet vertices, which are equidistant from each adjacent triplet of disks, and draw a circle about each of the vertices with a radius so that the circle just touches the three disks. If that radius is greater than the size of a disk, then an additional disk can adsorb within the circle. Evidently, they did not identify the actual triangle-shaped adsorption space, but picked points randomly in the circle that contained it—yet this was sufficient to reach the jamming limit in a reasonable amount of time. Their final result was that $\theta_J(\text{disks}) = 0.546 \pm 0.002$, and they also verified that (4) is followed. This procedure is (necessarily) rather intricate and time consuming, and the largest surfaces they considered adsorbed ≈ 2734 disks. A total of 35 simulations were carried out, yielding a total of $\approx 95\,700$ adsorbed disks.

III. RESULTS AND DISCUSSION

A. Jamming limit coverage

To determine the value of θ_J, $R = 44\,814$ runs were carried out on a 256×256 surface, where the unit length is the side of an adsorbing square. The x and y coordinates of the cells within each unit region of the surface were represented by a 31-bit integer, resulting in a discretization of $2^{31} \times 2^{31} \approx 4.6 \times 10^{18}$ points per unit area. A total of over 1.65×10^9 squares were adsorbed. We found

$$\langle N \rangle = 36\,831.81, \quad \sigma = 56.31 \tag{7}$$

where N is the number of adsorbed squares at the jamming limit and σ is the standard deviation in the sample of $R = 44\,814$ runs. The value of θ_J then follows as $\langle N \rangle / A$, where the area $A = 65\,536$, and the standard deviation of error in that estimate is $(\sigma / A)/\sqrt{R}$. Thus our final result is

$$\theta_J = 0.562\,009 \pm 0.000\,004\ , \tag{8}$$

where the uncertainty represents one standard deviation.

By the law of large numbers we would expect, for systems of different A,

$$\theta_J = \langle \theta_J \rangle \pm f/\sqrt{RA}\ , \tag{9}$$

where RA is proportional to the total number of squares that will adsorb in R runs, and f is a constant, independent of R and A. Comparison of (9) with (8) yields $f = 0.22$. The error predicted by this formula is generally consistent with the errors reported in other works. For example, Feder's work on parallel squares[11] consisted of $R = 5$ runs on a surface of area $A = 5000$. Equation (9) predicts an uncertainty in θ_J of 0.0014 for Feder's data. This is in rough agreement with the uncertainty of 0.002 reported by Feder.

B. Time dependence

At all stages of the program, the number of squares adsorbed on the surface was stored whenever the time increased by a factor of 2. These stored values were then averaged over different runs and the standard deviation calculated to get the final result. Part of the data collected for a system of area 256×256 is presented in Table I. To check Swendsen's prediction,[16] Eq. (3), we plot $\theta(t)$ versus $(\ln t)/t$ for $t \geq 128$ (Fig. 2). It can be seen that Swendsen's prediction falls within one standard deviation of the data for $t \gtrsim 6000$.

TABLE I. Coverage as a function of time for a 256×256 system.

$\log_2(t)$	θ_J
−15	$3.051\,757\,8 \times 10^{-5} \pm 0$
−12	$0.000\,244\,017\,7 \pm 6.4 \times 10^{-9}$
−8	$0.003\,875\,16 \pm 1.0 \times 10^{-7}$
−4	$0.055\,517\,5 \pm 1.3 \times 10^{-6}$
0	$0.329\,719\,2 \pm 4.0 \times 10^{-6}$
4	$0.512\,088\,5 \pm 3.6 \times 10^{-6}$
8	$0.554\,860\,0 \pm 3.9 \times 10^{-6}$
12	$0.561\,255\,0 \pm 4.0 \times 10^{-6}$
16	$0.561\,943\,0 \pm 4.1 \times 10^{-6}$
20	$0.562\,004\,1 \pm 4.1 \times 10^{-6}$
24	$0.562\,008\,5 \pm 4.1 \times 10^{-6}$
28	$0.562\,008\,8 \pm 4.1 \times 10^{-6}$
31	$0.562\,008\,8 \pm 4.1 \times 10^{-6}$

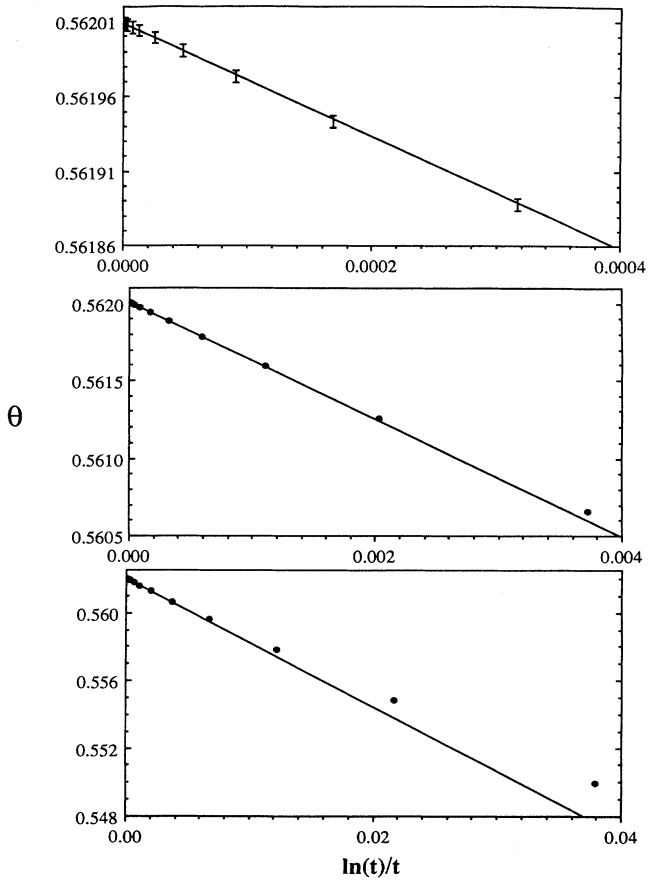

FIG. 2. Test of Swendsen's asymptotic dynamics. The line shown follows the equation $\theta(t)=0.562\,01-0.378\ln(t)/t$.

C. Surface size and discreteness effects on θ_J

The question arises of how the size and discretization of the absorbing surface effects the jamming coverage of the system. By "discretization of the surface" ($\equiv S^2$), we mean the number of lattice sites per unit area available to the center of an adsorbing square on an empty lattice. (There were $2^{31}\times 2^{31}$ sites per unit area in simulations discussed in the preceding two subsections). By "size of the surface" ($\equiv A$), we mean the total area of the adsorbing surface (256×256 in the simulations of the preceding two subsections). Blaisdell and Solomon[12] have investigated this topic for aligned square RSA onto a surface with hard boundary conditions. Their analysis is not applicable to our simulations due to our use of periodic boundary conditions.

Discreteness effects have been studied previously for one- and two-dimensional RSA. Mackenzie showed analytically[31] that for an infinite one-dimensional lattice the jamming coverage goes as

$$\theta_J(S)-\theta_J(\infty)=0.2162S^{-1}+0.0362S^{-2}+\cdots\ , \qquad (10)$$

where $S=1,2,3,\ldots$ is the number of lattice sites across a particle. In Table II we list jamming coverages for systems of aligned squares at various discretizations. The data were produced by simulations on a system of area $A=256\times 256$. We found that the data fit quite well to the equation

$$\theta_J(S)-\theta_J(\infty)=0.315S^{-1}+0.114S^{-2}\ . \qquad (11)$$

TABLE II. Jamming coverage as a function of S for a 256×256 system.

S	θ_J
2	$0.747\,943\pm 3.7\times 10^{-5}$
4	$0.647\,927\pm 2.2\times 10^{-5}$
8	$0.603\,355\pm 5.5\times 10^{-5}$
16	$0.582\,223\pm 3.9\times 10^{-5}$
32	$0.571\,916\pm 2.7\times 10^{-5}$
64	$0.567\,077\pm 4.0\times 10^{-5}$
128	$0.564\,405\pm 5.1\times 10^{-5}$
256	$0.563\,074\pm 5.2\times 10^{-5}$
512	$0.562\,647\pm 3.1\times 10^{-5}$
1024	$0.562\,346\pm 3.3\times 10^{-5}$
4096	$0.562\,127\pm 3.3\times 10^{-5}$
16 384	$0.562\,038\pm 3.3\times 10^{-5}$
2 147 483 648	$0.562\,008\,8\pm 4.1\times 10^{-6}$

Table II and Eq. (11) imply that the discretization used to determine (8) (the jamming coverage for a system with $S=2^{31}$) is far more than adequate.

Nakamura[19] also ran simulations to determine the effects of discretization on the jamming limit coverage. His results are in general agreement with (11). Evans[32] used a generalization of the Palasti conjecture[12,26] to discrete RSA to find the constants in (11), and found $\theta_J(S)-\theta_J(\infty)=0.323S^{-1}-0.007S^{-2}$. However, the Palasti conjecture is known to give the wrong result in the limit $S\to\infty$.

We have collected some preliminary data on the effect of surface size on θ_J. The value of θ_J was measured for surfaces of area $2^n\times 2^n$, where $n=2-10$. The measurements were made using an adsorbing surface with the maximum discretization ($S=2^{31}$). For 1×1 and 2×2 systems, the coverage is exactly 1. (The reader can verify that a 2×2 system with periodic boundary conditions will always achieve total coverage.) For the surface of area 4×4 we found $\theta_J=0.562\,305\pm 0.000\,006$. For each surface of area 8×8 and greater, the jamming coverage was calculated to a standard deviation of less than 0.000 02, and we found that these jamming coverages all had overlap with (8), the jamming coverage for a 256×256 system. Additionally, we calculated the coefficient f defined in (9), and found $f=0.22$ for all the runs except $n=2$ (4×4), where $f=0.09$. Thus, quite accurate values of θ_J can evidently by measured using simulations on a surface as small as 8×8. In the next subsection, we will show that this remarkable result is due to the rapid damping of the two-point correlation functions.

D. Two-point correlation functions

The two-point correlation function, $G(r,\alpha)$, is defined as the probability of finding an adsorbed square centered

in a neighborhood of (r,α), given that there is a square centered at the origin. Here r is the radial coordinate measured in lengths of the side of an adsorbing square, and α is the angular coordinate defined in Fig. 3. $G(r,\alpha)$ is normalized with the jamming limit coverage, so that at jamming $G(r,\alpha)\rightarrow 1$ as $r\rightarrow\infty$. Figure 3 shows the two-point correlation function for squares at the jamming limit. Note that $0\leq\alpha\leq\pi/4$ and $0\leq r\leq\infty$ covers all space, due to the fourfold symmetry of the problem. Values of $r\cos\alpha=1$ correspond to contact between two squares, and $r\cos\alpha=n+1$ correspond to the minimum distance between two square centers such that n squares can be placed between the first two squares. The two-point correlation functions diverge at $r\cos\alpha=1$, and have local minima at $r\cos\alpha=2$ and 3. (The minimum at 3 could not be conclusively detected for $\alpha=\pi/4$.)

Each curve in Fig. 3 crosses the line $G(r,\alpha)=1$ at $r\cos\alpha\approx 1.5$. Thus, there is a tendency of squares to form more "holes" of width under 0.5 than would be formed if the square centers were uniformly distributed. Additionally, squares are somewhat discouraged from forming holes of width slightly larger than 0.5. Notice that the divergence of $G(r,\alpha)$ at contact occurs more rapidly as α is decreased. Thus, if we know that a square center is going to fall within $r\cos\alpha<1.5$ of another square center, it is more likely that the two squares will achieve an orientation with a small α than an orientation with a large α. Given two squares separated by a "hole" somewhat larger than 0.5 (i.e., with $r\cos\alpha$ somewhat greater than 1.5), the two squares are more likely to have a relative orientation with large α than an orientation with small α.

Swendsen has stated[16] that for $\alpha=0$ the divergence of the two-point correlation function at contact should be the same as the divergence in one dimension:

$$G(r,0)=C_1\ln(r-1),\quad r\rightarrow 1 \tag{12}$$

with $C_1=-0.8434$.[31] Our data are consistent with the form

$$G(r,\alpha)=C_0+C_1\ln(r\cos\alpha-1)\ , \tag{13}$$

for $r\cos\alpha\rightarrow 1$, with values of C_0 and C_1 given for various α in Table III. In comparing (12) and (13) we note that the constant term of (13) will eventually be overwhelmed by the logarithmic term as $r\cos\alpha\rightarrow 1$, and (13) will approach (12). However, for $\alpha=0$, the constant term in (13) accounts for over 10% of the value of $G(r,\alpha)$ when $r-1$ is as small as 0.0005. Figure 4 shows the fit of the two-point correlation function to (13) for $\alpha=0$.

The two-point correlation-function data were collected using shells of size $\delta r=\frac{1}{200}$, and $\delta\alpha=\frac{1}{200}$ rad. When plotting the data of Fig. 3, we simply placed each data point at the midpoint of its respective shell. Thus the data for the shell $1<r<1.005$ were plotted at $r=1.0025$. The exact position of the data point within δr was not very important, due to the small size of δr. In Fig. 4, however, the positioning of the data point within the shell becomes very important for $r\rightarrow 1$, due to the divergence of

TABLE III. Coefficients for Eq. (13).

α	C_0	C_1
0	−1.97	−2.50
$\pi/16$	−0.05	−1.16
$\pi/8$	0.21	−0.84
$3\pi/16$	0.53	−0.53
$\pi/4$	0.99	−0.13

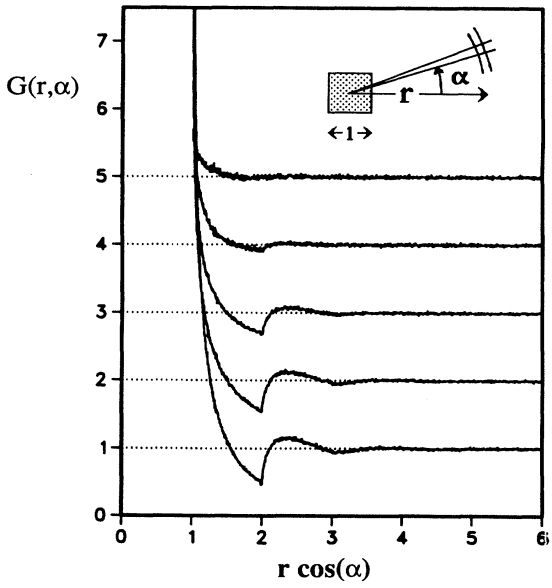

FIG. 3. Two-point correlation functions. The inset in the upper right shows how r and α are defined with respect to the adsorbed square at the origin. The curves are, from bottom to top, $\alpha=0$, $\pi/16$, $\pi/8$, $3\pi/16$, and $\pi/4$. Each successive curve is translated upward one unit.

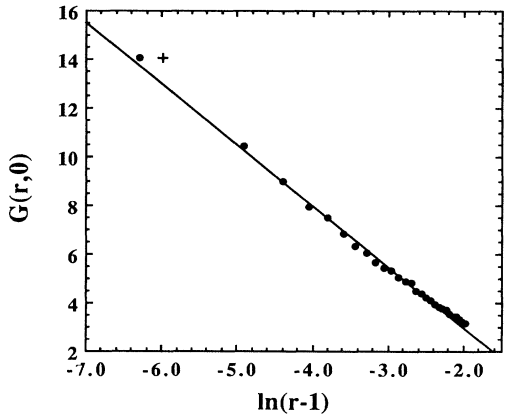

FIG. 4. The ●'s show the logarithmic divergence of the correlation function at contact for $\alpha=0$. The data shown are for $r-1\leq 0.135$. The line is a least-squares fit to the data, and follows the equation $G(r,\alpha)=-1.97-2.50\ln(r-1)$. The + shows the data plotted at the midpoint of the shell for $r_1=1$. For $r_1\geq 1.005$ there is almost no difference between $r_1+\delta r/2$ and r^* of Eq. (16).

$\ln(r-1)$ at $r=1$. For example, the data for the shell $1<r<1.005$ could naively be plotted anywhere in the region $-\infty<\ln(r-1)<-5.30$.

To determine the best value of r at which to plot each data point, we assumed a form for $G(r,\alpha)$ across each shell:

$$G(r,\alpha)=K_1+K_2\ln(r\cos\alpha-1)\ , \tag{14}$$

where K_1 and K_2 are arbitrary constants that may vary from shell to shell. Our program stores data only on $\bar{G}(r,\alpha)$, the average of $G(r,\alpha)$ across each shell:

$$\bar{G}(r,\alpha)=\frac{\int_{\alpha}^{\alpha+\delta\alpha}d\alpha\int_{r_1}^{r_1+\delta r}dr\,r\,G(r,\alpha)}{\int_{\alpha}^{\alpha+\delta\alpha}d\alpha\int_{r_1}^{r_1+\delta r}dr\,r}\ , \tag{15}$$

where the integration limits are the upper and lower bounds of the differential area element of interest. We wish to find the value of r^* at which $G(r^*,\alpha)=\bar{G}(r,\alpha)$. After making the change of variables $z=r\cos\alpha-1$, we find that r^* is determined by

$$\ln z^*=\frac{[\frac{1}{2}z^2\ln z-\frac{1}{4}z^2+z\ln z-z]_{r_1\cos\alpha-1}^{(r_1+\delta r)\cos\alpha-1}}{[\frac{1}{2}z^2+z]_{r_1\cos\alpha-1}^{(r_1+\delta r)\cos\alpha-1}}\ , \tag{16}$$

with $z^*=r^*\cos\alpha-1$, and with r_1 the lower bound of the shell. We used (16) to find the value of r^* at which to plot the data collected in the interval $(r_1, r_1+\delta r)$. Only the leftmost point in Fig. 4 had a value of r^* significantly different than the midpoint of its shell. Notice that K_1 and K_2 of Eq. (14) drop out and do not appear in (16).

Expanding (16) about δr for the "first" shell, $1<r\cos\alpha<1+\delta r$, one finds

$$r^*=\frac{1}{\cos\alpha}+\frac{\delta r}{e}+\frac{(\delta r)^2\cos\alpha}{4e}+O((\delta r)^3)\ , \tag{17}$$

which shows that to lowest order the data point should be plotted a distance $\delta r/e$ from the inside of the shell at $r_1=1/\cos\alpha$. Expanding (16) in the limit of $(r_1\cos\alpha-1)/\delta r\gg 1$ (i.e., for two squares far from contact), one finds

$$r^*=r_1+\tfrac{1}{2}\delta r+O((\delta r)^2)\ , \tag{18}$$

so that in this limit it is valid to plot the data point in the center of the radial interval.

We found it convenient to define a "box average" two-point correlation function, $G_{\rm box}[r,\alpha,\theta(t)]$. The box average correlation function is the probability of finding a square center located in a neighborhood of a square "box" of side length $2r$ centered at the origin, given that there is an adsorbed square centered at the origin (see Fig. 5). Again, $G_{\rm box}$ is normalized against the jamming limit coverage, so that $G_{\rm box}[r,\alpha,\theta(t)]\to\theta(t)/\theta_J$ as $r\to\infty$. Note that with the above definition of $G_{\rm box}$, $r=1$ corresponds to contract between two squares, and $r=2$ corresponds to the smallest distance between two squares such that a third square can be placed between the two. The box average correlation function has largely the

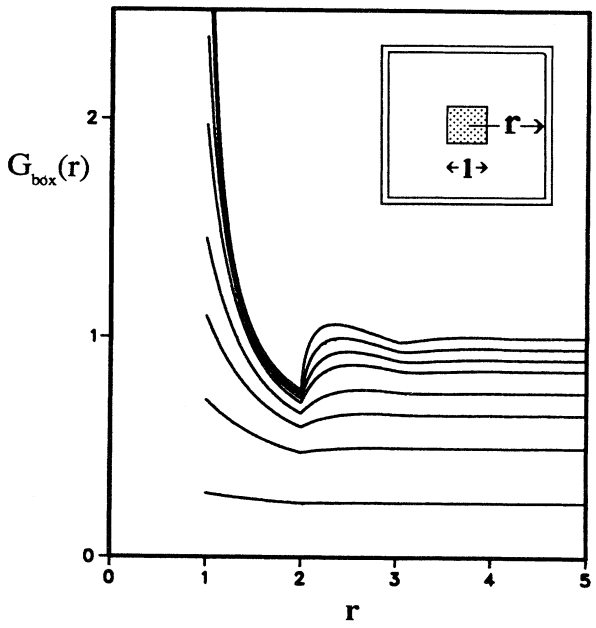

FIG. 5. The box average correlation function. The inset in the upper right corner shows a unit square at the origin and a neighborhood of a "box" of side length $2r$. The curves are, from bottom to top, $\theta(t)/\theta_J=0.25$, 0.50, 0.65, 0.75, 0.85, 0.90, 0.95, and 1.00.

same shape as the curves of Fig. 3. In Fig. 5 we have plotted the box average correlation function at various coverages. We note that places where the curves are spread far apart represent regions where adsorption is likely to occur for coverages between the coverage of the two curves. Likewise, places where curves bunch together represent regions where adsorption is unlikely. Hence, adsorption at $r=2$ is extremely unlikely at coverages over $\frac{3}{4}\theta_J$, while adsorption is much more likely at $r\approx 2\frac{1}{3}$ for these same coverages.

The data of Fig. 3–5 were generated on a surface of area 256×256, with a discretization of $2^{31}\times2^{31}$ lattice sites per unit area. The data were collected for each curve by averaging the individual radial distribution functions of over 15×10^6 squares in RSA configurations.

Although all squares that adsorb in a RSA process are in some sense identical to each other (in that each square has the same size and shape and follows the same rules for the failure or success of an adsorption), not all squares exhibit the same behavior. In particular, we found that squares that adsorbed late in the simulation were distinguishable (in a probabilistic sense) from squares that adsorbed early in the simulation. In Fig. 6 we show the box average correlation functions *at the jamming limit* for the first square to absorb, the last square to adsorb, and also for the square that adsorbed at a coverage of $\frac{3}{4}\theta_J$. All the correlation functions diverge at $r=1$; however, the correlation function for the last square to adsorb exhibits a much stronger divergence. Also, there is evidently a discontinuity in $G_{\rm box}$ at $r=2$ for the last square to ad-

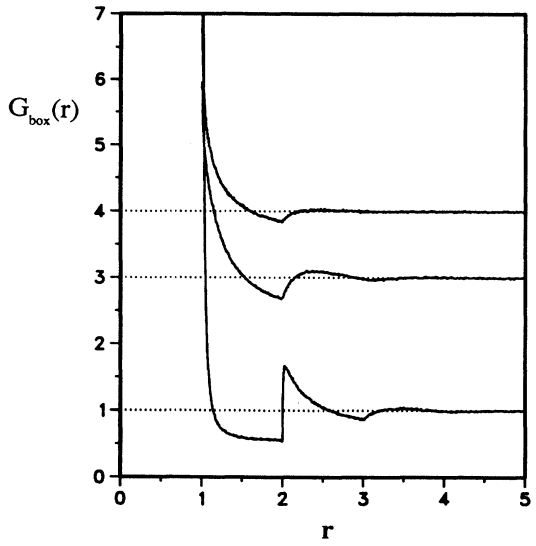

FIG. 6. The box average correlation function at the jamming limit for the last square to adsorb (bottom), the square to adsorb at $\frac{3}{4}\theta_J$ (middle), and the first square to adsorb (top). Each successive curve has been translated upward for clarity.

sorb, while there is a discontinuity only in the derivative of G_{box} for the other squares. Note that we determined the correlation functions for squares that adsorbed at $\frac{1}{4}\theta_J$ and $\frac{1}{2}\theta_J$, but these functions were so similar to the correlation function for the first square to adsorb that we did not include them in the figure.

The functions of Fig. 6 were generated from $R=5200$ runs on a 64×64 surface with a discretization of $2^{31}\times2^{31}$ lattice sites per unit area. The smaller surface was used because of the large number of runs needed to collect data of the sort presented in Fig. 6. The reason that more runs were needed to collect the data of Fig. 6 than to collect the data of Fig. 3–5 is that a jamming limit configuration provides $\theta_J A$ adsorbed squares on which to collect data for Fig. 3–5, but the same configuration provides only one "first square to adsorb" on which to collect data for Fig. 6.

IV. CONCLUSIONS

We have found that the RSA of parallel squares can be simulated to the jamming limit using a reasonable amount of computer time. This allowed us to calculate θ_J to unprecedented accuracy, and to calculate radial distribution functions precisely. We were even able to get good data for the radial distribution functions of squares that landed at specific coverages, even though attaining such data required that an entire adsorption be simulated to get data for only a single square.

Investigations were performed to discover the dependence of θ_J on the degree of discretization of the adsorbing surface. A similarity was found between the effects of discretizing the absorbing surface in one- and two-dimensional RSA. Further investigations might consider the effects of discretization on the dynamics of the adsorption. The discretization of the surface will determine the size of the smallest "hole" onto which a square can adsorb. Thus, the approach to jamming should be more rapid on a coarse lattice than on a fine lattice, due to the absence of very small "holes" on the coarse lattice. [Note that Swendsen's asymptotic dynamics (3) applies to a continuous surface, and predicts that the jamming limit will only be reached in the limit $t\rightarrow\infty$.]

Investigations were also performed to discover the dependence of θ_J on the size of the adsorbing surface. When periodic boundary conditions are used, the jamming limit coverage is found to be independent of surface size for surfaces of area $2^n\times2^n$ with n an integer greater than 2. Further investigations might consider the effects on θ_J of adsorbing surface sizes other than $2^n\times2^n$. We do not expect θ_J to vary for surfaces much larger than 8×8, due to the rapid damping of the two-point correlation functions. For smaller surfaces, however, we would expect θ_J to oscillate as the adsorbing surface area is increased. To see this, consider a 1×1 system, in which $\theta_J=1$. As the surface area A is increased, the coverage will decrease according to $\theta_J=1/A$, until at $A=2\times2$ exactly four squares always adsorb, and the jamming coverage jumps to exactly 1. As we increase the surface area again, the coverage will decrease according to $\theta_J=4/A$ until $A=3\times3$, at which point more than four squares can adsorb. For $A>3\times3$, the relationship between θ_J and A becomes more complicated. The preceding argument is valid only for square surfaces.

Swendsen's dynamics for long times were found to agree well with our simulated data for times $t\gtrsim6000$. Swendsen's prediction of a logarithmic divergence for the two-point correlation function at contact also agreed with our data.

The two-point correlation functions along constant α were shown to have similar shapes when $G(r,\alpha)$ is plotted against $r\cos\alpha$ for various α. It is possible that the only difference between the curves for various α is the rate at which the curves damp out. This similarity suggests the use of the box average correlation function. The large shell size of the box average correlation increases the ease with which correlation-function data can be collected.

Note added. While revising this paper, we received a copy of unpublished work from V. Privman, J. S. Wang, and P. Nielaba[33] that has some overlap with the work presented here. While their work deals primarily with the issue of the time dependence of RSA on a discrete lattice (i.e., small S), the authors also verified Swendsen's dynamics (3) for a continuous surface, although with less precision than we have achieved here. Additionally, they reported values of θ_J for small S that are in good agreement with the values we report in Table II.

ACKNOWLEDGMENTS

The authors acknowledge support from the U.S. National Science Foundation under Grant No. DMR-86-19731.

[1]J. D. Bernal, Nature (London) **183**, 141 (1959).
[2]P. J. Flory, J. Am. Chem. Soc. **61**, 1518 (1939).
[3]J. J. Gonzalez, P. C. Hemmer, and J. S. Høye, Chem. Phys. **3**, 228 (1974).
[4]A. Rènyi, Magy. Tud. Akad. Mat. Kut. Intéz, Közl. **3**, 109 (1958) [Sel. Transl. Math. Stat. Prob. **4**, 203 (1963)].
[5]Y. Pomeau, J. Phys. A **13**, L193 (1980).
[6]H. Solomon, in *Proceeding of the Fifth Berkeley Symposium on Mathematics, Statistics, and Probability,* edited by J. Neyman (University of California Press, Berkeley, 1966), Vol. 3, p. 119.
[7]E. L. Hinrichsen, J. Feder, and T. Jøssang, J. Stat. Phys. **44**, 793 (1986).
[8]P. Schaaf and J. Talbot, Phys. Rev. Lett. **62**, 175 (1989).
[9]J. W. Evans, Phys. Rev. Lett. **62**, 2642 (1989).
[10]M. Tanemura, Ann. Inst. Stat. Math. **31B**, 351 (1979).
[11]J. Feder, J. Theor. Biol. **87**, 237 (1980).
[12]B. E. Blaisdell and H. Solomon, J. Appl. Prob. **7**, 667 (1970).
[13]Y. Akeda and M. Hori, Nature (London) **254**, 318 (1975).
[14]Y. Akeda and M. Hori, Biometrica **63**, 361 (1976).
[15]W. S. Jodrey and E. M. Tory, J. Stat. Comp. Sim. **10**, 87 (1980).
[16]R. H. Swendsen, Phys. Rev. A **24**, 504 (1981).
[17]J. Talbot, G. Tarjus, and P. Schaff, Phys. Rev. A **40**, 4808 (1989).
[18]R. D. Vigil and R. M. Ziff, J. Chem. Phys. **91**, 2599 (1989), and J. Chem. Phys. (to be published).
[19]M. Nakamura, J. Phys. A **19**, 2345 (1986) 1021 (1987).
[20]L. Finegold and J. T. Donnell, Nature (London) **278**, 443 (1979).
[21]G. C. Barker and M. J. Grimson, Mol. Phys. **63**, 145 (1988).
[22]E. Burgos and H. Bonadeo, J. Phys. A **20**, 1193 (1987).
[23]J. W. Evans and R. S. Nord, Phys. Rev. B **31**, 1759 (1985).
[24]P. Meakin, J. L. Cardy, E. Loh, Jr., and D. J. Scalapino, J. Chem. Phys. **86**, 2380 (1987).
[25]L. A. Rosen, N. A. Seaton, and E. D. Glandt, J. Chem. Phys. **85**, 7359 (1986).
[26]I. Palásti, Magy. Tud. Akad. Mat. Kut. Intéz. Közl. **5**, 353 (1960).
[27]*Handbook of Mathematical Tables,* edited by M. Abramowitz and I. A. Stegun (Dover, New York, 1980).
[28]W. G. Hoover and A. de Rocco, J. Chem. Phys. **36**, 3141 (1962).
[29]F. van Swol, Mol. Sim. **1**, 95 (1987).
[30]B. Widom, J. Chem. Phys. **44**, 3888 (1966); **44**, 4043 (1973).
[31]J. K. Mackenzie, J. Chem. Phys. **37**, 723 (1962).
[32]J. W. Evans, J. Phys. A **20**, 3063 (1987).
[33]V. Privman, J. S. Wang, and P. Nielaba (unpublished).